# Intensity-dependent two-electron emission dynamics with orthogonally polarized two-color laser fields

Zongqiang Yuan,[1] Difa Ye,[1] Qinzhi Xia,[1] Jie Liu,[1,2] and Libin Fu[1,2,*]

[1]*Institute of Applied Physics and Computational Mathematics, Beijing 100088, China*

[2]*HEDPS, Center for Applied Physics and Technology, Peking University, Beijing 100084, China*

(Received 27 February 2015; published 23 June 2015)

In this paper, we explore the intensity-dependent strong-field double ionization of Ne with orthogonally polarized two-color laser pulses consisting of 800- and 400-nm laser fields. The yield of $Ne^{2+}$ as a function of the relative phase $\Delta\phi$ of the two colors experiences a qualitative transition as the laser intensity decreases from the saturation regime to the far-below-saturation regime. In the saturation regime, our simulations well reproduce the recent experimental observations [Phys. Rev. Lett. **112**, 193002 (2014)]. Turning to the far-below-saturation regime, however, we find that the observed small knee structure totally disappears and the maximum yield of $Ne^{2+}$ is shifted by a $\pi/2$ phase. This is explained by the competition between the trajectory concentration effect and the $\Delta\phi$-dependent ionization rate of the tunneling electron. The possibility of controlling over the two-electron emission direction along the 400-nm field through the laser intensity is also investigated. We show that the two-electron emission direction can be reversed by changing the laser intensity for some vales of $\Delta\phi$, while this fails for some other values of $\Delta\phi$.

DOI: 10.1103/PhysRevA.91.063417 PACS number(s): 32.80.Rm, 42.50.Hz, 32.80.Fb

## I. INTRODUCTION

Nonsequential double ionization (NSDI) of atoms in strong laser field can trace its history back to the first observation of the knee structure on the doubly charged ionization curve of Xe atoms as a function of the laser intensity [1]. The mechanism of NSDI has been investigated intensively for more than three decades and the electron recollision picture is now accepted broadly [2,3]. Despite the great progress on NSDI, new experimental phenomena still constantly emerge and challenge our existing knowledge. Recent examples include the striking anticorrelated electron emission for Ar below the recollision threshold [4], the cross-shaped structure in the correlated two-electron momentum spectrum along the laser polarization direction with near-single cycle laser pulses [5], and the nonstructured momentum distribution of strong-field double ionization of high-$Z$ rare-gas atoms [6].

In recent years, the orthogonally polarized two-color (OTC) laser pulses have captured the attention of the strong-field community due to their broad applications, such as the generating of clean high-harmonic spectrum [7–9], the steering of the electrons with subfemtosecond precision [10–12], the tomographic reconstruction of molecular orbitals [13,14], and the directional proton emission in dissociation of molecules [15]. More recently, the OTC pulses were used to investigate experimentally atomic double ionization close to the saturation regime of $Ne^{+}$ [16]. The possibilities to control the electron-electron correlation and their emission directions are demonstrated by tuning the subcycle shape of the electric field of the OTC pulses. Yet the measured yield of $Ne^{2+}$ as a function of the relative phase $\Delta\phi$ substantially deviates from the predictions of the Ammosov-Delone-Krainov (ADK) tunneling theory, indicating the important role of the interparticle Coulomb interaction competing with the strong laser field. Simulations based on a two-dimensional (2D) semiclassical model including all interactions qualitatively explain the experimental results. The investigation, however, is confined to a laser intensity close to the saturation regime. How the laser intensity will affect the NSDI in OTC pulses has not been studied there. We note that the subcycle control of the correlated electron emission may have potential applications in chemical reactions. Hence it should be interesting to further study the intensity dependence, and other aspects as well, of NSDI for the cases of OTC pulses.

In this paper, with a full three-dimensional (3D) semiclassical model, we extend the investigations in Ref. [16] to explore in more detail the intensity dependence of the double ionization of Ne with the OTC pulses. Our calculations cover a wide range of laser intensities from the saturation regime to the far-below-saturation regime [17]. In the saturation regime, our simulations agree with the recently observed $\Delta\phi$-dependent $Ne^{2+}$ yield, faithfully reproducing the positions of the maximum and the minimum as well as a small knee structure [16]. However, as the laser intensity decreases deeply into the far-below-saturation regime, the original small knee structure totally disappears and the maximum yield of $Ne^{2+}$ is shifted by a $\pi/2$ phase. To explain this completely different behavior, we extend a theory in which forces acting on the electrons come only from the laser field, once the electrons have become free in some way. This approach, first proposed by van Linden van den Heuvell and Muller [18], has been repeatedly applied for nearly 30 years in discussions of high-field ionization. Furthermore, we find that the two-electron emission direction along the second-harmonic field axis can be changed by varying the laser intensity for some values of $\Delta\phi$. However, for some other values of $\Delta\phi$, the two electrons emit with fixed direction independent of the laser intensity. The complex relative phase and laser intensity dependent two-electron emission dynamics is uncovered by the subcycle dependence of the electron recollision time.

The rest of this paper is organized as follows. We first introduce our 3D semiclassical model in Sec. II. Section III is devoted to the yield of the doubly charged ion $Ne^{2+}$. In

*lbfu@iapcm.ac.cn

 

Sec. IV, correlated two-electron emission is explored and the underlying mechanism is revealed by analyzing the subcycle dynamics of classical trajectories. Finally, we conclude our paper in Sec. V. Atomic units (a.u.) are used throughout the paper unless specified otherwise.

## II. 3D SEMICLASSICAL MODEL

We consider a two-active-electron atom interacting with OTC pulses of the form $\vec{E}(t) = \epsilon_x f_x(t)\cos(\omega t)\vec{e}_x + \epsilon_z f_z(t)\cos(2\omega t + \Delta\phi)\vec{e}_z$, with $\Delta\phi$ the relative phase of the two colors. The OTC pulses combine an 800-nm laser pulse, frequency $\omega$, field amplitude $\epsilon_x$, and its second harmonic pulse, frequency $2\omega$, field amplitude $\epsilon_z$, polarized along the $x$ and $z$ directions, respectively. $f_x(t)$ and $f_z(t)$ are the envelope functions. One electron is released at the outer edge of the field-suppressed Coulomb barrier along the combined-field direction through quantum tunneling with a rate given by the ADK tunneling theory [19]. The tunneled electron has a Gaussian distribution on the transverse velocity and zero longitudinal velocity [20–23]. The bound electron is sampled from a microcanonical distribution [24]. The subsequent evolution of the two electrons with the above initial conditions is governed by Newton's equations of motion: $\frac{d^2\vec{r}_i}{dt^2} = -\vec{E}(t) - \nabla_{r_i}(V^i_{ne} + V_{ee})$. Here, index $i$ denotes the two different electrons. $V^i_{ne} = -\frac{2}{|\vec{r}_i|}$ and $V_{ee} = \frac{1}{|\vec{r}_1 - \vec{r}_2|}$ are Coulomb interactions between nucleus and electrons and between two electrons, respectively. In our calculations, the laser peak intensity in either color is $I_{800\,\mathrm{nm}} = I_{400\,\mathrm{nm}} = (0.2\text{–}1.0)\times 10^{15}$ W/cm$^2$, covering both the saturation and far-below-saturation regime. For even lower laser intensities, the tunneling rate would cease to be a pertinent quantity since the Keldysh parameter is close to one meaning that nonadiabatic transitions (multiphoton transitions) become dominant. The OTC laser field has a constant amplitude for the first eight cycles and is turned off with a three-cycle ramp of the 800-nm field. The first and second ionization potentials are chosen as $I_{p1} = 0.79$ a.u. and $I_{p2} = 1.51$ a.u. to match the neon atom. $5\times 10^7$ trajectories, with different ADK rates and initial conditions, have been launched for each intensity and relative phase resulting in statistically convergent results for comparison.

## III. YIELD OF THE DOUBLY CHARGED ION

### A. Trajectory concentration effect

Figure 1(a) presents the intensity dependence of the yield of $Ne^{2+}$ as a function of the relative phase $\Delta\phi$. At the highest intensity, the yield of $Ne^{2+}$ depends on $\Delta\phi$ with maxima around $\Delta\phi = (n + 0.5)\pi, n \in \mathbb{N}$ and small knee structures around $\Delta\phi = n\pi, n \in \mathbb{N}$ [black line with squares in Fig. 1(a)]. While this picture substantially changes as the decrease of the laser intensity, i.e., the small knee structures get enhanced and the maximum yields of $Ne^{2+}$ move to $\Delta\phi = n\pi, n \in \mathbb{N}$ [magenta line with left triangles in Fig. 1(a)].

To understand the transition behavior mentioned above, we first make statistics on the number of trajectories that eventually lead to double ionization. As shown in Fig. 1(b), for all intensities, the number of DI trajectories $N_{\mathrm{DI}}$ strongly

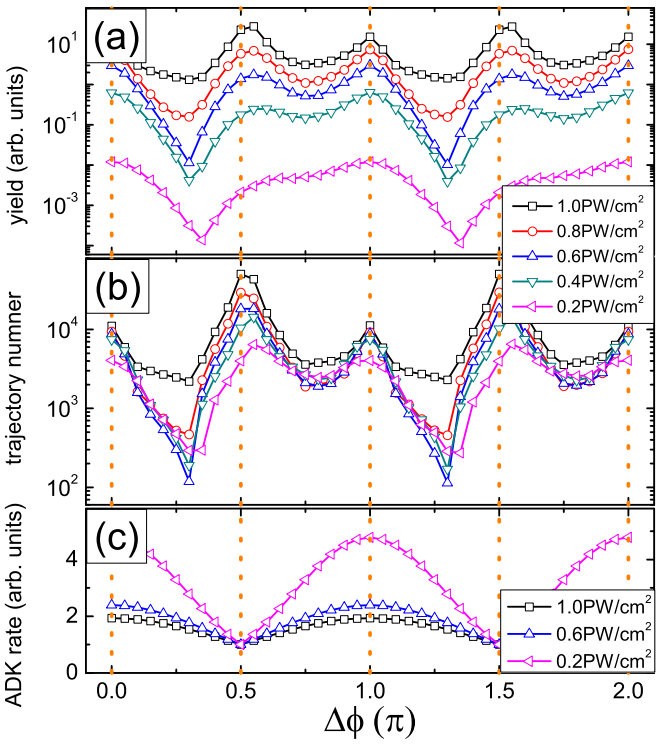


FIG. 1. (Color online) (a) Yield of $Ne^{2+}$ as a function of the relative phase $\Delta\phi$ at intensities of $(0.2\text{–}1.0)\times 10^{15}$ W/cm$^2$. (b) The same as (a) but for the number of trajectories that eventually lead to double ionization. (c) Ionization rates of the tunneling electrons released at the field maxima (calculated with the ADK theory [19]).

depends on $\Delta\phi$ with maxima around $\Delta\phi = (n + 0.5)\pi$, $n \in \mathbb{N}$ and small knee structures around $\Delta\phi = n\pi, n \in \mathbb{N}$. This universal behavior, independent of the laser intensity, is coined as trajectory concentration effect in the following, indicating that by tuning the relative phase of the OTC pulses the number of DI trajectories can be astonishingly increased by as much as two orders of magnitude. Because the yield of $Ne^{2+}$ is the product of the number of DI trajectories and their corresponding weights given by the tunnel ionization rate, thus the transition behavior in Fig. 1(a) is attributed to the competition between the $\Delta\phi$-dependent $N_{\mathrm{DI}}$ and the $\Delta\phi$-dependent tunnel ionization rate of the first electron.

At the highest intensity, the tunnel ionization rate varies relatively slowly as $\Delta\phi$ changes [black line with squares in Fig. 1(c)] indicating that the laser intensity is in the saturation regime; therefore, the dependence of $Ne^{2+}$ yield on $\Delta\phi$ has an analogous trend as that for $N_{\mathrm{DI}}$, i.e., with maxima around $\Delta\phi = (n + 0.5)\pi, n \in \mathbb{N}$ and small knee structures around $\Delta\phi = n\pi, n \in \mathbb{N}$. In the far-below-saturation regime, however, the tunnel ionization rate is much more sensitive to the field maximum as modulated by $\Delta\phi$ [magenta line with left triangles in Fig. 1(c)], and thus it dominates the features of the $\Delta\phi$ dependence of the yield of $Ne^{2+}$, which maximizes around $\Delta\phi = n\pi, n \in \mathbb{N}$, the same as the tunnel ionization rate.

Our simulation results in the saturation regime qualitatively agree with the experimental results of Ref. [16]. We should mention that the experiment was performed at a laser intensity of $I_{800\,\mathrm{nm}} = I_{400\,\mathrm{nm}} = (2 \pm 0.2)\times 10^{14}$ W/cm$^2$, which as claimed in Ref. [16] is close to the saturation regime.

We predict a different saturation threshold intensity. The reason could be twofold. First, the focus volume effect is not considered in our model. Secondly, in the experiment, the accurate determination of laser peak intensity is still an open question. Both aspects hamper the quantitative comparison of experimental data with theoretical results that sensitively depend on the laser intensity. However, we emphasize that the qualitative picture drawn by our simulation, putting aside the exact value of saturation intensity, is fully consistent with the experiment, i.e., if our simulation is in the saturation regime defined by our model and the experiment data is in the saturation regime verified by the experiment itself, then the results are similar. Moreover, our predictions in the far-below-saturation regime can be easily verified in current experiment by decreasing the experimental intensity.

### B. Mechanisms of the trajectory concentration

In this subsection, we explain why the number of double ionization trajectories $N_{\mathrm{DI}}$ shows qualitatively the same behavior for all intensities as presented in Fig. 1(b) and explore the origin of the experimentally observed small knee structures [16]. This is facilitated by a simplest analytical model, which is a generation of the theory first proposed by van Linden van den Heuvell and Muller [18]. Suppose that the first electron tunnels out at the instant of field maximum $t = t_0$, with the initial position and velocity taken to be zero and neglecting the influence of the Coulomb interactions, the motion of the tunneled electron is solely determined by the OTC laser field and thus can be solved analytically,

$$x(t) = \frac{\epsilon_x}{\omega^2}[\cos(\omega t) - \cos(\omega t_0) + \omega(t - t_0)\sin(\omega t_0)], \quad (1)$$

$$z(t) = \frac{\epsilon_z}{4\omega^2}[\cos(2\omega t + \Delta\phi) - \cos(2\omega t_0 + \Delta\phi) + 2\omega(t - t_0)\sin(2\omega t_0 + \Delta\phi)]. \quad (2)$$

Figures 2(a)–2(f) demonstrate several typical trajectories of the tunneled electron given by Eqs. (1) and (2) as $\Delta\phi$ increases. The red star in each plot marks the position where the tunneling electron becomes locally closest with the original point after its first departure, with $R_0$ denoting the distance to the origin. The corresponding time difference from tunneling to the closest approach is defined as the travel time. The $\Delta\phi$ dependence of the travel time (left axis) and $R_0$ (right axis) are shown in Fig. 2(g). Due to the periodicity, we confine our following analysis to the region $\Delta\phi \in [0.5\pi, 1.5\pi]$.

The travel time is pivotal in the recollision scenario of NSDI. Due to the initial transverse velocity of the tunneled electron, long travel time results in the rapid decrease of the recollision probability. In addition to the initial transverse velocity, the electron also has a phase-dependent drift velocity, which again strengthens the importance of the travel time. Meanwhile, large value of $R_0$ is the second reason which leads to the decrease of the recollision probability. From Fig. 2(g), we see that the travel time attains its minimum at $\Delta\phi = 0.5\pi$, where $R_0$ is relatively small. This explains the trajectory concentration effect, i.e., the maximum of $N_{\mathrm{DI}}$ at $\Delta\phi = 0.5\pi$ as shown in Fig. 1(b). As $\Delta\phi$ increases from $0.5\pi$ to $1.5\pi$, the travel time increases monotonically, reaches the maximum at $\Delta\phi = \pi$, and keeps constant thereafter. This

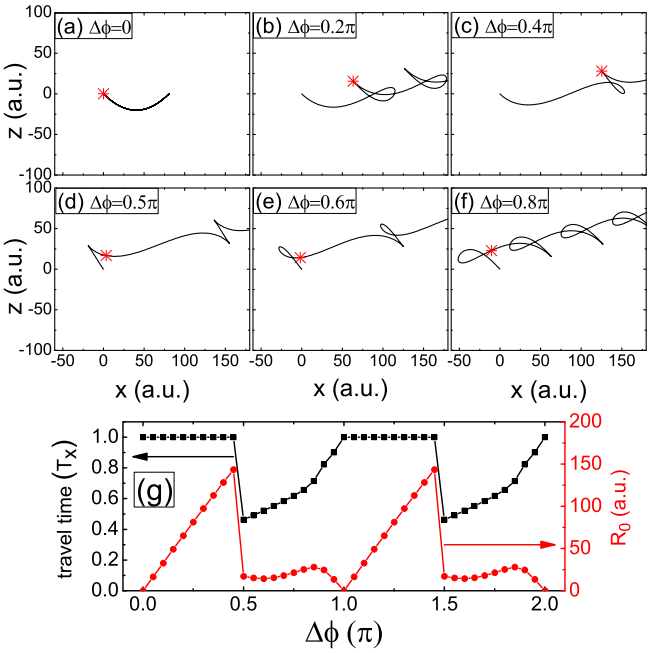


FIG. 2. (Color online) (a)–(f) Trajectories of the tunneled electron for several typical values of $\Delta\phi$ according to Eqs. (1) and (2). The red stars mark the closest approach of tunneling electron to the origin; see the text for detail. (g) Travel time and $R_0$ as a function of $\Delta\phi$. The laser peak intensity is $I_{800\,\mathrm{nm}} = I_{400\,\mathrm{nm}} = 6\times10^{14}$ W/cm$^2$. $T_x$ denotes the optical period of the 800-nm laser field.

is the reason for the overall decreasing tendency of $N_{\mathrm{DI}}$ in the interval $[0.5\pi, 1.3\pi]$. Inspecting the behavior around $\Delta\phi = \pi$, one finds that, whereas the travel time reaches the maximum, $R_0$ becomes a minimum. The competition between these two factors gives rise to the small knee structures as shown in Fig. 1(b) and observed in Ref. [16]. Based on the proceeding arguments, we claim that the rather intuitive simplest analytical model is able to catch and to explain almost all the main features of the $\Delta\phi$-dependent doubly charged ion yield observed in experiment.

## IV. TWO-ELECTRON EMISSION DYNAMICS

### A. Momentum distribution of the doubly charged ion

In addition to the subcycle shape of the OTC pulses (controlled by the relative phase $\Delta\phi$), intensity of the laser pulses is another important ingredient to manipulate the two-electron emission dynamics. In experiment, the momentum spectrum of $Ne^{2+}$ along the 400-nm direction exhibits a pronounced $\Delta\phi$-dependent asymmetry in the emission direction [16]. We present the same results in Fig. 3 and extend them to three typical laser intensities to show how laser intensity provides additional control over the two-electron emission direction. In the saturation regime, our simulation [Fig. 3(a)] again well reproduces the experimental observations [Fig. 2(b) in Ref. [16]], i.e., the doubly charged ions acquire a sinusoidally oscillating mean momentum [Fig. 3(b)] with maximum yield at $\Delta\phi = 0.5\pi$ and $1.5\pi$ [Fig. 3(a)]. As the laser intensity decreases, the oscillation period increases roughly to three over $2\pi$ phase [Fig. 3(f)],

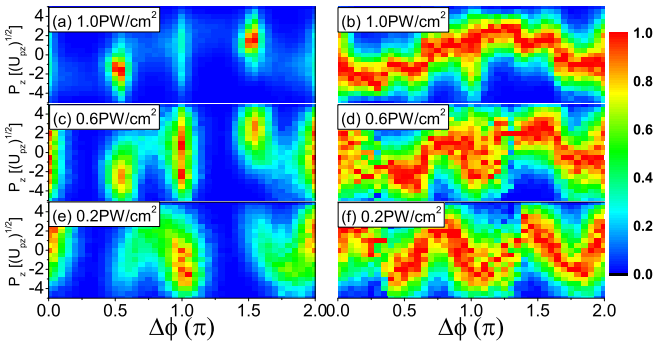


FIG. 3. (Color online) Momentum distributions of $Ne^{2+}$ along the polarization direction of the 400-nm laser field as a function of $\Delta\phi$ at intensities of (a) $10^{15}$ W/cm$^2$, (c) $6\times10^{14}$ W/cm$^2$, and (e) $2\times10^{14}$ W/cm$^2$. The distribution is normalized with respect to the maximum in each plot. Panels (b), (d), and (f) are the same as (a), (c), and (e), respectively, but normalized individually with respect to the maximum at each $\Delta\phi$, making the oscillation patterns more clearly visualized.

and the maxima move to $\Delta\phi=\pi$ and $2\pi$ [Fig. 3(e)]. It indicates that the control over the two-electron emission direction is more effective in the far-below-saturation regime, i.e., a relatively small change of $\Delta\phi$ can realize the control.

### B. Correlated two-electron momentum spectrum

Detailed insight into the two-electron emission dynamics can be obtained by the correlated two-electron momentum spectrum. We present the spectra along the 400-nm direction in Fig. 4 at three typical $\Delta\phi$. For each $\Delta\phi$, the laser intensity takes the values from $10^{15}$ W/cm$^2$ to $2\times10^{14}$ W/cm$^2$ with a decreasing step of $2\times10^{14}$ W/cm$^2$. We start our discussions from Fig. 4(A1) at $\Delta\phi=0$ in the saturation regime. The momentum distribution mainly occupies the first quadrant, which means that both electrons are emitted dominantly into the same hemisphere with positive momentum. The ratio of first- over third-quadrant distribution gradually decreases as the decrease of the laser intensity (first row in Fig. 4, from left to right) and finally the momentum distribution mainly occupies the third quadrant in the far-below-saturation regime [Fig. 4(A5)]. These results indicate that we can control the directionality of the parallel emission of the two electrons through laser intensity. Integrating the spectra over the lines $p_{z,\mathrm{ion}}=-(p_{1z}+p_{2z})$, one obtains the momentum distribution of $Ne^{2+}$, which is expected to exhibit a single-hump structure located at a negative value in the saturation regime, converting to a double-hump structure in the medium regime, and then again a single-hump structure located at a positive value in the far-below-saturation regime, entirely consistent with early results presented in Fig. 3. The picture significantly changes for the case of $\Delta\phi=0.5\pi$. As shown in Figs. 4(B1)–4(B5), the momentum distribution mainly occupies the second and forth quadrants in the saturation regime and converges to the first quadrant in the far-below-saturation regime, indicating the transition from the dominance of back-to-back emission to the dominance of side-by-side emission. For $\Delta\phi=0.75\pi$, the momentum distribution always mainly occupies the third quadrant [Figs. 4(C1)–4(C5)], independent of the laser intensity. These very different laser-intensity-dependent behaviors of the correlated two-electron momentum spectrum account for the different oscillation patterns on the momentum distribution of $Ne^{2+}$ shown in Fig. 3.

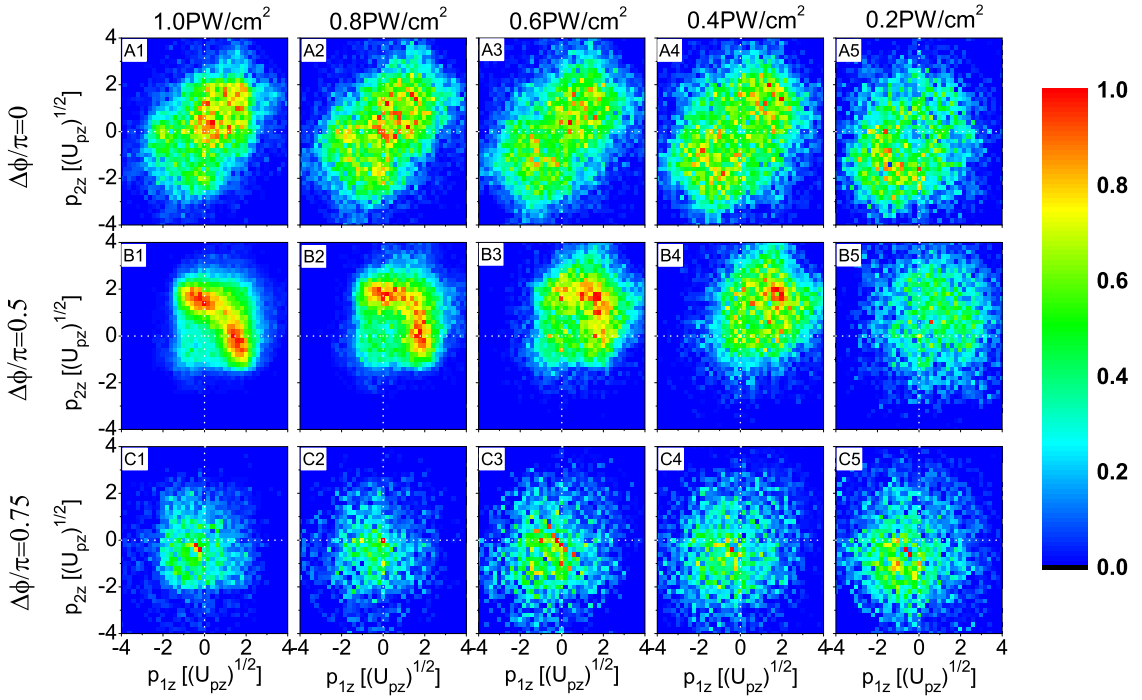


FIG. 4. (Color online) Probability contour plots of the correlated two-electron momentum spectrum along the 400-nm polarization direction at three typical relative phases: 0 (top row), $0.5\pi$ (middle row), and $0.75\pi$ (bottom row). Note that, in each plot, the results have been symmetrized along the diagonal of $p_{1z}=p_{2z}$ and then scaled to unity at the highest yield.

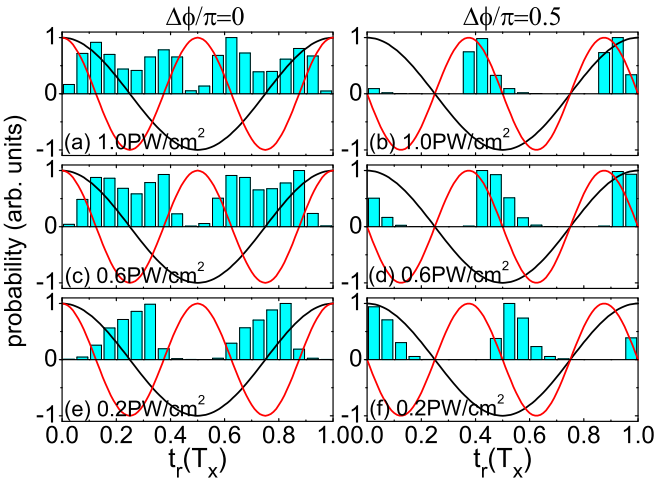


FIG. 5. (Color online) Probability distributions of the recollision time for $\Delta\phi = 0$ (left column) and $\Delta\phi = 0.5\pi$ (right column) at three typical laser intensities. The black and red solid curves represent the 800-nm and 400-nm laser fields, respectively.

### C. Subcycle dynamics

Analyzing the subcycle dynamics of the classical trajectories is highly beneficial to explaining the correlated two-electron momentum spectrum. We trace back the evolution of those trajectories that eventually lead to double ionization and present the probability distributions of the recollision time $t_r$ for $\Delta\phi = 0$ and $\Delta\phi = 0.5\pi$ as shown in the left and right columns of Fig. 5, respectively. Here, $t_r$ is defined as the instant of the closest approach of the two electrons, which is expressed in units of $T_x$ and has been translated within one through $t_r \to t_r - [t_r]$, with $[t_r]$ denoting the integer part of $t_r$. For $\Delta\phi = 0$, the distribution of the recollision time spans over a wide range of laser period, becoming narrower as the laser intensity decreases. Meanwhile, the peak moves from the falling edge (around $T_x/8$) to the rising edge (around $3T_x/8$) of the 400-nm laser field. For $\Delta\phi = 0.5\pi$, the recollision time only locates in the falling edge (around $T_x/2$) of the 400-nm laser field and is much narrower than that for $\Delta\phi = 0$. If both electrons ionize immediately after the recollision, the expected drift momentum along the 400-nm direction that two electrons gain from the laser field are given by $p_z = -A_z(t_r)$, where $A_z$ denotes the vector potential of the 400-nm field. This simple relationship provides a link between the experimentally observable momentum and the microscopic parameter $t_r$, explaining the structural changes in the momentum spectra on one hand, and offering the possibility to timing the recollision and ionization with attosecond resolution on the other hand [25,26].

## V. CONCLUSION

In summary, we have systematically investigated the relative phase and laser intensity dependence of the double ionization of Ne atoms irradiated by the OTC pulses. The qualitative transition of $Ne^{2+}$ yield as a function of the relative phase $\Delta\phi$ is revealed as laser intensity decreases from the saturation regime to the far-below-saturation regime, which is explained by the competition between the trajectory concentration effect and the $\Delta\phi$-dependent tunnel ionization rate. The underlying mechanism of the formation of the small knee structures observed in the saturation regime is explained with the help of the simplest analytical model. Correlated two-electron momentum spectrum along the 400-nm field is analyzed in detail and the possibility of controlling over the two-electron emission direction through laser intensity is explored. Our predictions might stimulate further experiments along this direction.

## ACKNOWLEDGMENTS

This work is supported by the National Basic Research Program of China (973 Program) (Grants No. 2013CBA01502, No. 2011CB921503, and No. 2013CB834100), the National Natural Science Foundation of China (Grants No. 11374040, No. 11274051, No. 11304018, No. 11404027, and No. 11475027), and the Foundation of President of the China Academy of Engineering Physics (Grant No. 2014-1-029).

[1] A. l'Huillier, L. A. Lompre, G. Mainfray, and C. Manus, Phys. Rev. A **27**, 2503 (1983).
[2] P. B. Corkum, Phys. Rev. Lett. **71**, 1994 (1993).
[3] W. Becker, X. Liu, P. J. Ho, and J. H. Eberly, Rev. Mod. Phys. **84**, 1011 (2012), and references therein.
[4] Y. Liu, S. Tschuch, A. Rudenko, M. Dürr, M. Siegel, U. Morgner, R. Moshammer, and J. Ullrich, Phys. Rev. Lett. **101**, 053001 (2008).
[5] B. Bergues, M. Kübel, N. G. Johnson *et al.*, Nat. Commun. **3**, 813 (2012).
[6] X. Sun, M. Li, D. Ye *et al.*, Phys. Rev. Lett. **113**, 103001 (2014).
[7] I. J. Kim, C. M. Kim, H. T. Kim, G. H. Lee, Y. S. Lee, J. Y. Park, D. J. Cho, and C. H. Nam, Phys. Rev. Lett. **94**, 243901 (2005).
[8] C. M. Kim and C. H. Nam, J. Phys. B **39**, 3199 (2006).
[9] L. Brugnera, D. J. Hoffmann, T. Siegel, F. Frank, A. Zaïr, J. W. G. Tisch, and J. P. Marangos, Phys. Rev. Lett. **107**, 153902 (2011).
[10] M. Kitzler and M. Lezius, Phys. Rev. Lett. **95**, 253001 (2005).
[11] L. Brugnera, F. Frank, D. J. Hoffmann *et al.*, Opt. Lett. **35**, 3994 (2010).
[12] Y. Zhou, C. Huang, Q. Liao *et al.*, Opt. Lett. **36**, 2758 (2011).
[13] D. Shafir, Y. Mairesse, D. M. Villeneuve, P. B. Corkum, and N. Dudovich, Nat. Phys. **5**, 412 (2009).
[14] H. Niikura, N. Dudovich, D. M. Villeneuve, and P. B. Corkum, Phys. Rev. Lett. **105**, 053003 (2010).
[15] X. Gong, P. He, Q. Song, Q. Ji, H. Pan, J. Ding, F. He, H. Zeng, and J. Wu, Phys. Rev. Lett. **113**, 203001 (2014).
[16] L. Zhang, X. Xie, S. Roither *et al.*, Phys. Rev. Lett. **112**, 193002 (2014).
[17] P. Dietrich, N. H. Burnett, M. Ivanov, and P. B. Corkum, Phys. Rev. A **50**, R3585 (1994).
[18] See H. B. van Linden van den Heuvell and H. G. Muller, in *Multiphoton Processes*, edited by S. J. Smith and P. L. Knight (Cambridge University Press, Cambridge, UK, 1988),

where they give the name "Simpleman" theory to this classical description in which only the laser force is utilized. Such a theory is one in a class of theories of electrons in plane-wave radiation fields. For a review, see J. H. Eberly, in *Progress in Optics*, edited by E. Wolf (North-Holland, Amsterdam, 1969), Vol. 7, p. 359.

[19] M. V. Ammosov, N. B. Delone, and V. P. Krainov, Zh. Eksp.Teor. Fiz. **91**, 2008 (1986) [Sov. Phys. JETP **64**, 1191 (1986)].

[20] J. Chen, J. Liu, L. B. Fu, and W. M. Zheng, Phys. Rev. A **63**, 011404(R) (2000).

[21] L. B. Fu, J. Liu, J. Chen, and S. G. Chen, Phys. Rev. A **63**, 043416 (2001).

[22] L. B. Fu, J. Liu, and S. G. Chen, Phys. Rev. A **65**, 021406(R) (2002).

[23] D. F. Ye, X. Liu, and J. Liu, Phys. Rev. Lett. **101**, 233003 (2008).

[24] J. G. Leopold and I. C. Percival, J. Phys. B **12**, 709 (1979).

[25] N. Camus, B. Fischer, M. Kremer *et al.*, Phys. Rev. Lett. **108**, 073003 (2012).

[26] D. F. Ye, J. Chen, and J. Liu, Phys. Rev. A **77**, 013403 (2008).